Novel Imaging Techniques in Cardiac Ion Channel Research

14

Esperanza Agullo-Pascual, Alejandra Leo-Macias, Donna R. Whelan, Mario Delmar, and Eli Rothenberg

Abstract

Light microscopy has long been at the forefront of biological research, perhaps most significantly in the form of fluorescence microscopy. This technique, paired with the ongoing discovery and synthesis of increasingly brilliant fluorophores, allows for visualization of the internal machinations of cells with molecular specificity. However, until recently, a persistent limitation of fluorescence microscopy—the diffraction of visible light—has restricted elucidation of the subcellular organization and localization of molecules to spatial resolutions of 200–300 nanometers. The invention and implementation of several super-resolution fluorescence microscopies (SRFMs) over the last 10 years have circumvented this diffraction limit and allowed up to tenfold improvements in resolution. Applications of SRFM in cardiology research have already illuminated aspects of the cardiac nanoscale architecture which were previously unobservable, opening the door for new avenues of research. These discoveries include the sub-diffraction structure of the intercalated disk, the t-tubular network, and excitation-contraction coupling. In this chapter we will review SRFM methodologies, present some examples of their successful application in cardiac research, and discuss the techniques' advantages, ongoing challenges, and future potential.

E. Agullo-Pascual · A. Leo-Macias · M. Delmar
The Leon H Charney Division of Cardiology, New York University School of Medicine, New York, NY, USA
e-mail: esperanza.agullo-pascual@nyumc.org; alejandra.leo-macias@nyumc.org; mario.delmar@nyumc.org

D. R. Whelan · E. Rothenberg (✉)
Department of Biochemistry and Molecular Pharmacology, New York University School of Medicine, New York, NY, USA
e-mail: donna.whelan@nyumc.org; eli.rothenberg@nyumc.org

D. Thomas, C. A. Remme (eds.), *Channelopathies in Heart Disease*, Cardiac and Vascular Biology 6, https://doi.org/10.1007/978-3-319-77812-9_14

Abbreviations

CLEM	Correlative light-electron microscopy
FP	Fluorescent protein
LM	Light microscopy
PALM	Photoactivation localization microscopy
SIM	Structured illumination microscopy
SMLM	Single-molecule localization microscopy
SRFM	Super-resolution fluorescence microscopy
STED	Stimulated emission depletion microscopy
STORM	Stochastic optical reconstruction microscopy

14.1 Introduction

Although the inventor of the compound microscope is a lingering point of contention, simple optical microscopes became available sometime in the seventeenth century, and in 1665 Robert Hooke coined the word "cell" and published what many consider to be the first important work on microscopy, *Micrographia*, a book which included illustrations of different microscopically examined specimens. Following this, single high-magnification lenses and compound microscopes were popularized as a technique for biologists by other scientists including Antonie van Leeuwenhoek and Marcello Malpighi. This soon allowed for the discovery and characterization of numerous previously undetectable organisms and cells such as bacteria, muscle fibers, and erythrocytes.

However, the technical difficulties of improving seventeenth-century microscopes, in particular due to problems with lens development and configuration, severely hindered further applications. Then, during the second half of the nineteenth century, Ernst Abbe described the principles of image formation in light microscopy and developed various new and improved lenses, and August Köhler invented Köhler illumination allowing for even sample illumination, adjustable contrast, and exclusion of the illumination source. This led to a breakthrough in the design and manufacturing of commercially available microscopes and reinstated optical microscopy as the key tool of biologists.

Following this, fluorescence microscopy was developed, with fluorophore discovery and synthesis, alongside labeling approaches, taking center stage. The first major advancement was the production and application of fluorescently labeled antibodies by Albert Coons in 1941 that enabled labeling of various cellular structures with bright synthetic fluorophores. This was followed in the 1990s by the utilization of the green fluorescence protein (GFP) as a fusion tag for live-cell imaging, which in turn catalyzed the development of a plethora of other FPs spanning the visible spectrum. Together, these advances allow for the fluorescent visualization of the subcellular landscape with, importantly, multiplexed molecular

specificity. However, despite these improvements in labeling, as well as technological improvements to the microscopes themselves, fluorescence imaging remained limited by the diffraction of visible light, a physical reality of the wave nature of photons described by Ernst Abbe in the nineteenth century. Diffraction limited the best possible spatial resolution of light microscopy to no better than a few hundred nanometers, causing blurriness in images and dictating hundreds of nanometers of uncertainty to molecular localizations and structures.

Recently, however, a revolution in fluorescence microscopy occurred with the development of techniques, collectively known as super-resolution fluorescence microscopy (SRFM), which circumvent the diffraction limit. This is achieved in one of two ways: either deterministically by structuring the illumination light or by stochastically imaging, and thus localizing, fluorophores individually. The importance of these novel technologies was recently recognized with the Nobel Prize in Chemistry in 2014.

SRFM has instigated a new era in fluorescence microscopy in which molecular specificity can now be paired with molecular localization. This allows for visualization of nanoscale architecture providing insight into the organization, orientation, and interactions of biomolecules in complex structures such as the synaptic button in neurons (Tang et al. 2016; Wilhelm et al. 2014; Dani et al. 2010), focal adhesions (Case et al. 2015; Kanchanawong et al. 2010), and nuclear pores (Loschberger et al. 2014; Szymborska et al. 2013).

Here we describe the different SRFM techniques available and review some of the applications of these methods in cardiac research. We also discuss SRFM limitations, other applications, and future potential.

14.2 Methods

SRFM encompasses several techniques which can broadly be classified as either relying on a deterministic approach which uses spatially patterned illumination light or on a stochastic approach which detects single fluorophores. Both (1) structured illumination microscopy (SIM) and (2) stimulated emission depletion microscopy (STED) are popular examples of the former, whereas (3) single-molecule localization microscopy (SMLM) describes several variants of the latter.

14.2.1 Structured Illumination Microscopy

SIM is a widefield approach which relies on the structuring of light using a grid pattern which generates a sinusoidal excitation pattern of known spatial frequency, orientation, and phase. The grid is rotated in steps to acquire different images that are processed to extract high-frequency information and produce a reconstructed image with a twofold improvement in lateral resolution (~100 nm) (Fig. 14.1) (Langhorst et al. 2009).

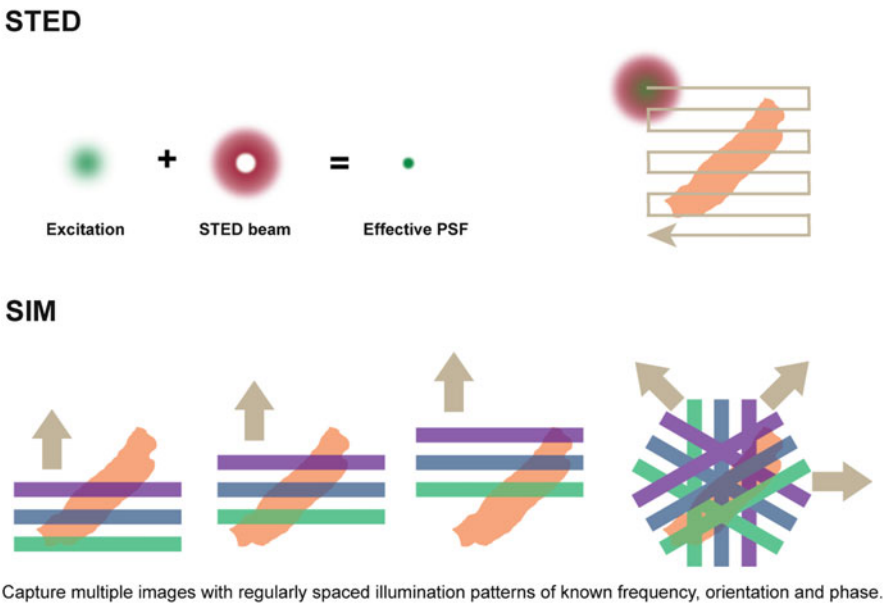

Fig. 14.1 An overview of the STED and SIM approaches to SRFM

While SIM setups have been available for longer than both STED and SMLM, there are relatively few published studies that use SIM to study cardiac architecture. In one of these studies, Granzier et al. labeled different regions of the protein Titin to study the role of the I-band/A-band junction on the strain on the molecular spring elements, uncovering biomechanical sensing associated with cardiac hypertrophy (Granzier et al. 2014). In another study, Lukyanenko et al. used SIM to localize Ca^{2+} /calmodulin-activated phosphodiesterase type 1A (PDE1) in sinoatrial nodal cells (Lukyanenko et al. 2016). This study shows that PDE1 localizes beneath the cell surface in sinoatrial nodal cells, an observation which provides insight into mechanisms for maintaining Ca^{2+} signaling and pacemaker function.

14.2.2 Stimulated Emission Depletion Microscopy

STED microscopy also relies on introducing patterns into the illumination light, but instead of a grid arrangement as in SIM, STED couples a conventional confocal illumination pattern with an overlapping torus-shaped "depletion" beam. Fluorophores illuminated by this depletion beam, i.e., those located away from the center of the focused confocal excitation beam, undergo stimulated emission and do not fluoresce. Consequently, any detected photons are known to originate in the sub-diffraction area where the torus beam does not overlap the excitation beam (Hell and Wichmann 1994). By raster scanning a sample with these two overlapping lasers using discrete acquisition steps of sub-diffraction size (usually 10–20 nm), a super-

resolution image can be obtained without any further processing (Fig. 14.1). The lateral resolution that can be achieved with this technique ranges from 20 to 70 nm and is dependent on the intensity and size of the depletion beam, as well as the scanning step size.

Because of its commercial availability, live-cell applicability, and compatibility with many conventional fluorophores, STED microscopy has been used in several investigations into cardiac cell architecture and molecular organization. In a study published by Wagner and colleagues, STED microscopy was used to image t-tubular organization in live cardiomyocytes and to follow remodeling after myocardial infarction (Wagner et al. 2012). The improved image resolution allowed detection of enlargement of the t-tubule cross sections as well as network-wide remodeling. These changes in the t-tubule morphology could explain the early excitation-contraction uncoupling observed during heart failure development after myocardial infarction.

STED was also used to unravel the molecular mechanisms of atrial fibrillation (AF) in research by Macquaide et al. which visualized the organization of the ryanodine receptor (RyR) in atrial myocytes (Macquaide et al. 2015). Analysis of these images revealed that although there was no change in RyR cluster size, the distance between clusters was reduced in AF. It was also found that RyR clusters grouped into Ca^{2+} release units (CRUs) were bigger and contained more RyR, although CRU organization (ratio RyR: total area per CRU) was more fragmented in AF myocytes. Moreover, the frequency of CRU along the z-line, as well as between z-lines, was increased in AF. Together these observations suggest that the probability of CRU firing and propagated Ca^{2+} release in AF could be increased, which would correlate with a higher Ca^{2+} spark frequency and duration.

The organization of ion channels at the intercalated disk has also been investigated using a modified version of STED microscopy called gated STED (gSTED). Veeraraghavan et al. described in two papers the distribution of sodium channels ($Na_V1.5$) (Veeraraghavan et al. 2015) and potassium channels ($K_{ir}2.1$) (Veeraraghavan et al. 2016) in the connexin43 (Cx43) gap junction perinexus area. gSTED differs from conventional STED microscopy in that it takes into consideration the fluorescence lifetime of detected emitters. Although the STED depletion beam cannot deplete all fluorophores outside the center of the excitation ring, it does affect the lifetimes of these fluorophores, thus providing a useful means of excluding erroneous emissions and allowing improved spatial resolutions. gSTED of guinea pig tissue sections and neonatal rat ventricular myocytes demonstrated that approximately one third of $Na_V1.5$ and $K_{ir}2.1$ clusters localize within 200 nm of a Cx43 cluster (perinexus area). These results, combined with some functional data and mathematical modeling, suggest that the perinexus is a specialized nanodomain surrounding the gap junction plaque, which plays a role in the propagation of electrical excitation via ephaptic transmission.

14.2.3 Single-Molecule Localization Microscopy

SMLM encompasses dozens of methods which all make use of stochastic single-molecule fluorescence emission and localization to construct super-resolution images. In 2006 three groups independently published the first SMLM methods: stochastic optical reconstruction microscopy (STORM) (Rust et al. 2006), photoactivation localization microscopy (PALM) (Betzig et al. 2006) and fluorescence PALM (FPALM) (Hess et al. 2006). These methods, along with the variations that followed, take advantage of the intrinsic photophysics of fluorophores which allow switching between emissive and dark states or between different absorption/emission wavelengths. In taking control of this switching, single fluorophores in densely labeled areas can be imaged individually by switching all surrounding fluorophores to a dark state or different color. This can be achieved with small synthetic fluorophores by inducing a reduced state via the semi-stable triplet state, or in fluorescent proteins via bleaching, or by several other photophysical/photochemical means (Reid and Rothenberg 2015). This on/off blinking behavior (rate of transition and "off" state duration) is different for each fluorophore and nanoscale cellular environment, and so optimization of fluorophore blinking must be achieved empirically through a combination of irradiation intensity, fluorophore concentration, and buffer conditions (e.g., oxidizing agents, reducing agents, and aqueous oxygen).

Once good fluorophore blinking is achieved, to obtain a super-resolved image, many thousands of frames are acquired with a different subset of fluorophores stochastically switched "on" in each frame. These movies are then processed using single-molecule emission finding and fitting algorithms which can determine, to within a few nanometers precision, the locations of each individual fluorophore (Fig. 14.2).

In particular, the direct STORM (*d*STORM) (Heilemann et al. 2008) imaging approach which makes use of many commercially available antibody-conjugated fluorophores has found much use in biological research including applications to elucidate macromolecular complexes in cardiac cells. Soeller and colleagues have focused on the organization of the ryanodine receptor in several papers (Baddeley et al. 2009; Hou et al. 2015; Wong et al. 2013). In their SMLM imaging, they demonstrated for the first time that RyR clusters vary widely in both shape and size. Interestingly, edge-to-edge distances showed that most of the clusters were within a distance of less than 100 nm with neighboring clusters suggesting the potential formation of "superclusters" that could facilitate the coupling of these receptors and trigger Ca^{2+} release cascades. Further studies have looked at the interaction of junctophilin-2 with RyR (Jayasinghe et al. 2012; Munro et al. 2016) and the Na^{+}/Ca^{2+} exchanger (NCX) (Wang et al. 2014). De La Fuente et al. also performed super-resolution imaging of the mitochondrial calcium uniporter in cardiac mitochondria, demonstrating its association to the sarcoplasmic reticulum and RyR clusters (De La Fuente et al. 2016).

Our group has further taken advantage of the improved resolution of SRFM to probe the molecular architecture of the intercalated disk in cardiomyocytes. In our

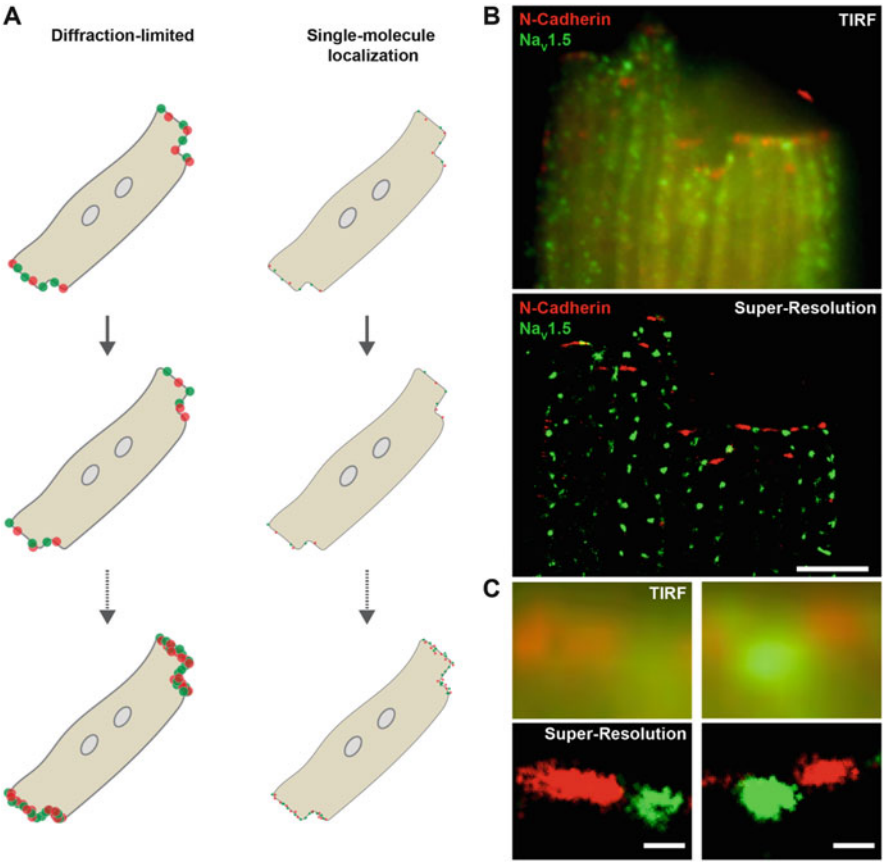

Fig. 14.2 Single-molecule localization microscopy. (**a**) Illustration of data acquisition for SMLM. Only a subset of fluorophores are in the "on" state in each frame allowing localization of each single molecule with nanometer accuracy. (**b**) An isolated adult mouse cardiomyocyte stained for N-cadherin (red) and $Na_V1.5$ (green). The top panel shows a TIRF image (diffraction-limited), while the bottom panel shows the super-resolved image of the same cell with improved resolution. (**c**) Zoom regions of B show the enhanced spatial resolution achieved by SMLM. Scale bars: 5 μm (**b**), 400 nm (**c**)

first study, we demonstrated that Cx43 and plakophilin-2 (PKP2), molecules that pertain to gap junctions and desmosomes, respectively, also interact at the membrane in neonatal cardiomyocytes (Agullo-Pascual et al. 2013). Moreover, when silencing the anchoring protein ankyrin-G, this interaction was reduced, and Cx43 organization was altered. These observations were further supported by Monte-Carlo simulations that demonstrated that the detected cluster overlaps were not random but a functional event. Follow-up studies continued to investigate the interactions between the different complexes that localize at the intercalated disk such as Cx43/gap junctions with sodium channels ($Na_V1.5$) (Agullo-Pascual et al. 2014) and PKP2 with $Na_V1.5$ (Cerrone et al. 2014). The nanoscale resolution obtained with *d*STORM images allowed us to look at the organization and interaction between proteins as

well as trafficking to the intercalated disk. Furthermore, the decreased sodium current measured by patch clamp in cardiomyocytes from these mice (Cx43D378stop (Agullo-Pascual et al. 2014) and PKP2-Hz[30]) correlated with a decrease in both the number of $Na_V1.5$ clusters and the number of microtubule plus-end protein EB1 clusters at the intercalated disk.

So far, we have only discussed the highlighted SRFM methodologies in their 2D super-resolution capabilities and applications because in the vast majority of SRFM research, only lateral imaging is undertaken or required. 3D modifications are available; however, they are often more complicated to implement and use and inevitably suffer from decreased temporal resolution and increased data handling and storage difficulties, two problems which are already limiting to 2D SRFM. Nonetheless, visualization of 3D organization can be key to an experiment, and so, in some cases, the trade-off is deemed necessary. In these cases, 3D-SIM is usually the most approachable because it is inherently a three-dimensional approach, needing only for the grated illumination pattern to be oriented axially as well. Furthermore, most commercial SIM microscopes are outfitted with both software and hardware for 3D imaging. Similarly, because of its confocal excitation scheme, STED can be used to produce 3D data simply by producing z-slices, albeit with diffraction limited z-resolutions. Alternatively, sub-diffraction axial resolutions can be realized by applying a second depletion beam which depletes fluorophores away from the center of the illumination beam in xz space.

In SMLM methodologies, many different approaches have been described for generating 3D data; in particular, these efforts have focused on manipulation and examination of single-molecule emission patterns [point spread functions (PSFs)] to encode and extract axial position information. For example, interferometric PALM uses two objectives and imaging paths allowing for the same photon to travel two paths and then recombine and self-interfere. The difference in distance traveled by the photon along the two paths is dependent on the fluorophore's axial position which can thus be calculated from the detected difference in phase amplitude of the self-interfering photon and the unaffected photon (Shtengel et al. 2009). Structures like focal adhesions and microtubules have been resolved in three dimensions at the nanometer scale using this approach (Case et al. 2015; Kanchanawong et al. 2010; Shtengel et al. 2009).

Biplane 3D also employs two imaging paths, introducing a slight difference in the distance between the objective and two cameras so that PSFs appear with different intensities and sizes (Proppert et al. 2014). More recently, algorithms have been put forward to extract z-information from 2D SMLM data, with the caveat that the distance from the imaging plane deduced is not identifiable as above or below (Franke et al. 2017). Huang et al. proposed an astigmatic approach to achieving 3D-SMLM in which a weak cylindrical lens is introduced into the emission path to distort the PSF in a predictable fashion based on axial position. Fluorophores above the imaging plane appear elongated along one lateral axis, while those below the imaging plane appear elongated in the other lateral axis (Huang et al. 2008). The ratio of the PSF size in the two axes can then be used with a calibration curve of known z-position PSF xy ratios to construct a 3D image (Fig. 14.3).

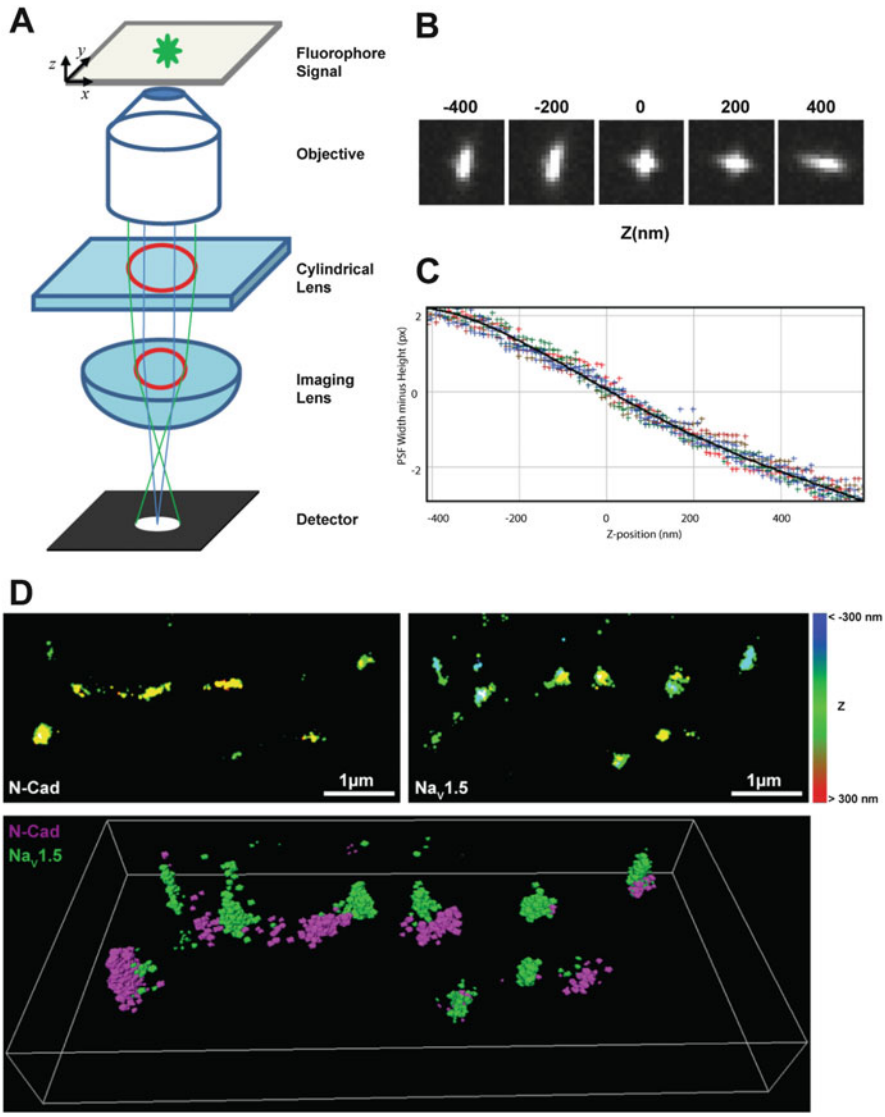

Fig. 14.3 Three-dimensional SMLM by astigmatism. (**a**) Diagram of 3D-SMLM system. (**b**) Examples of astigmatic images of a 100 nm diameter fluorescent bead in different axial positions. (**c**) A calibration curve used to generate 3D-SMLM images. The z-position is determined by the width minus height of the point spread function (PSF). (**d**) 3D-SMLM image of the cell end of an isolated adult mouse cardiomyocyte stained for N-cadherin (magenta) and $Na_V1.5$ (green). Top images show a 2D z-color coded image of N-cadherin (left) and of $Na_V1.5$ (right). Bottom image shows the 3D view of the same region

Using astigmatic 3D-SMLM, the periodic actin/spectrin cytoskeletal structure in axons has been discovered (Xu et al. 2013). Our group has also used this method to describe the distribution of sodium channels at the intercalated disk and their relation to adhesion molecules (Leo-Macias et al. 2016). Using two-color 3D super-resolution, we found that 35% of $Na_V1.5$ clusters co-localized with, or were within 100 nm of, N-cadherin clusters. Moreover, analysis of the cluster dimensions demonstrated a correlation with the predicted dimensions measured by angle view patch clamp. These observations lead us to speculate that the presence of adhesion/excitability nodes at the intercalated disk facilitates cross talk between the contractile and electrical apparatus.

14.3 Correlative SMLM and Electron Microscopy

Conventional fluorescence microscopy allows protein imaging in living cells with high molecular specificity but without significant insight into their ultrastructural context. Electron microscopy, on the other hand, provides a high level of detail at the ultrastructural level but is lacking in molecular specificity and multiplex capability. Because the strengths of these techniques are exceptionally complementary, their combination in correlative light-electron microscopy (CLEM) has the potential to fill many gaps in biological imaging research. Indeed, successful CLEM studies, especially those that make use of SRFM, have demonstrated the ability to precisely localize specific proteins within the highly detailed ultrastructural landscapes of their native cellular contexts.

Many protocols for CLEM have been developed in recent years, but the technique remains challenging due to differences in sample preparation requirements for fluorescence microscopy and EM (Johnson et al. 2015; Paez-Segala et al. 2015).

One particular example of CLEM is the visualization of $Na_V1.5$ ion channels. These were imaged in relation to the adhesion protein N-cadherin within the ultrastructural context of thin sections of ventricular tissue (Fig. 14.4) (Leo-Macias et al. 2016). After SMLM imaging of the ion channel and adhesion proteins, the sample was processed for, and imaged using, transmission electron microscopy (TEM). The SMLM and EM images were overlaid using fiducial markers visible in both images, allowing specific selection and further study of those $Na_V1.5$ clusters located at the membrane of the end-to-end contact of the cardiac cells, the so-called intercalated disc. Further analysis of these regions revealed that $Na_V1.5$ preferentially aggregates with the adhesion molecule N-cadherin. The combination of this result with electrophysiology and adhesion strength experiments demonstrated that these clusters are major contributors to cardiac sodium current and that loss of $Na_V1.5$ expression reduces intercellular adhesion. These adhesion/excitability nodes are proposed to be key sites for cross talk of the contractile and electrical molecular apparatus and may represent the structural substrate of cardiomyopathies in patients with mutations in molecules of the VGSC complex, as was the case in this report (Te Riele et al. 2017).

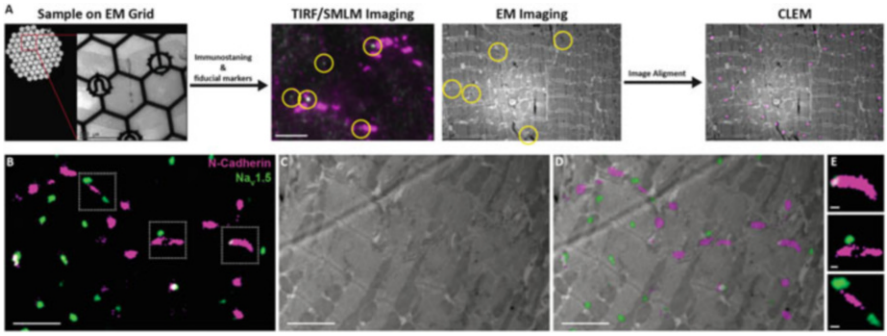

Fig. 14.4 Correlative light—electron microscopy. (**a**) Protocol for CLEM. Sample is mounted on an EM finder grid. After immunolabeling and addition of fiducial markers, the sample is imaged first for SMLM and then further processed for EM imaging. The same imaged region can be localized using the features on the grid, and the images are aligned using the fiducial markers that can be detected on both images. (**b**–**d**) Detection of N-cadherin (magenta) and $Na_V1.5$ (green) in a mouse heart tissue section by CLEM. (**e**) Zoom regions at the intercalated disk show localization of adhesion molecules and sodium channels in close apposition. Scale bar: 5 μm (**a**), 2 μm (**b**–**d**), 200 nm (**e**)

14.4 Advantages of SMLM and Ongoing Challenges

The SRFM approaches described here offer imaging capabilities that surpass the diffraction limit of light, but each comes with its own advantages and limitations. While SIM provides only a twofold improvement in resolution (lateral resolution of 120 nm) and is technologically complex, the availability of commercial instruments and its ease of use makes the technique approachable. This is particularly true when one takes into account the interchangeability of conventional fluorescence microcopy samples with SIM samples: any conventional fluorophore can be used, and live-cell imaging is constrained only by temporal resolution. Given the resolution provided in SIM, it is therefore recommended only when studying big cellular complexes like sarcomeres (Granzier et al. 2014). In comparison, STED and SMLM offer resolutions well below 100 nm that allow the study of molecular interactions and complexes, but despite commercial instruments being available and homebuilt instrumentation relatively straightforward (especially for SMLM), both methods suffer from more complicated sample preparations. STED relies on extremely resilient fluorophores which can be depleted but do not easily bleach or blink, while SMLM requires dyes which can be manipulated to blink. In both cases, the dyes must fulfill the requirements of the imaging methodology while also integrating into the sample with high specificity and, especially in the case of live cells, minimal perturbation to the sample. Of the available SRFMs, SMLM is arguably the most widely used (Huang et al. 2009), and so below we will primarily focus on the specifics of SMLM.

Despite its increasing number of applications, SMLM remains an emerging, highly specialized method, and several considerations need to be taken into account in order to perform a successful experiment. Optimization of sample preparation and imaging conditions are among the most important steps. This is because all nonspecific fluorophore labeling and sample degradation during fixation and imaging will result in false-positive localizations in the final SMLM image, as will low signal to noise and overlapping single molecule blinks. Furthermore, while the localization precision of SMLM data relies predominantly on the number of photons detected in a single-fluorophore signal, the spatial resolution relies not only on the precision but also the labeling type and degree of success and is strongly impacted by the presence of any imaging artifacts. Apart from nonspecific labeling, many of these artifacts come from suboptimal fluorophore blinking, which can be affected by several parameters:

- Imaging buffer: The blinking properties of fluorophores arise from electronic and structural changes in dye molecules. In many respects it is a stochastic process that arises from the recurring transition of the emitter between a non-emissive state (off) and an emissive state (on). A table of the most prevalent SMLM fluorophores is provided in Table 1 in Reid and Rothenberg (2015). For many conventional organic fluorophores, the off state is achieved by reduction of the semi-stable triplet state by an added reductant such a mercaptoethylamine. Return to the emissive on state is often caused by collision of dark reduced fluorophores with aqueous oxygen, and so controlling its concentration can also control blinking kinetics. This can be achieved by addition of an oxygen scavenging system, the most common of which comprises of glucose, glucose oxidase, and catalase. An added advantage of oxygen scavenging is that aqueous oxygen is responsible for some irreversible photobleaching events which are also undesired in SMLM experiments.
- Laser intensity: The number of cycles per second of fluorophores, between the ground and excited electronic states as achieved by photon absorption, vibrational relaxation, and photon emission, is largely dependent on photon flux. The probability of transition of an excited fluorophore to the semi-stable triplet state from which it can be reduced and stably switched off is stochastic, and so the probability of such a transition occurring in a given time also correlates directly with laser intensity. In contrast, laser intensity does not largely affect the probability of an off to on transition over a given time.
- Signal to noise ratio: In SMLM it is important to detect as many photons as possible from a single fluorophore in order to localize the molecule with nanometer precision. Therefore, overlapping PSFs, out-of-plane fluorescence, and autofluorescence can all interfere with the successful detection and localization of single molecules. In order to improve signal to noise, a total internal reflection fluorescence (TIRF) or highly inclined and laminated optical sheet (HiLo) configuration can be implemented. Both techniques angle the incident light so that only a fraction of the sample interacts with the incident light, thereby removing noise from out-of-plane fluorescence. In TIRF, an evanescent wave is used to

excite fluorophores within only a few hundred nanometers of the coverslip, while HiLo can be adjusted to excite fluorophores across variable depths of several microns.

– Labeling density: To achieve ultrastructural insight using SMLM, very high labeling densities must be used as described by the Nyquist sampling theory. Simply put, to achieve a true spatial resolution of x nm, a fluorophore must be localized every $x/2$ nm in the target structure. If SMLM is being used to quantify single-molecule distributions or interactions, it is similarly very important to achieve a high degree of labeling so as to not underestimate interactions. By altering acquisition parameters, namely, laser intensity and the concentrations of reductant and molecular oxygen, very densely labeled samples can be manipulated to optimize the ratio of fluorophores in the dark state to those in the emissive state. Over-labeling of samples for SMLM therefore only occurs when increased antibody aggregation and nonspecific labeling are observed.

Ideal SRFM experimental conditions vary widely depending on the target of interest, the fluorophores used, and the sample itself; therefore, extensive and careful optimization must be undertaken for each new experiment (Whelan and Bell 2015).

Analysis and rendering of SMLM data present a further challenge despite the availability of dozens of free software suites, ImageJ plug-ins, and open access codes [for a summary and comparison of algorithms, see Sage et al. (2015)]. Each of these analytical tools attempts to detect and localize each single-molecule emission within a data set, thus generating a list of coordinates which can be rendered into an "image." Most of these approaches can be distilled into three steps: first, detection of a potential single-molecule emission, usually by searching for local maxima; second, determination of the precise localization of the single-molecule emitter by fitting a Gaussian or arbitrary PSF; and finally rendering of the localized coordinates in 2D or 3D space. Various degrees of complexity and flexibility exist within and between the algorithms. Denoising (e.g., band/low-pass filtering and wavelet transformation) and thresholding can be used to process the raw data for detection of single-molecule emissions, while localization can be achieved using least squares, maximum likelihood, center of mass, or center of symmetry methods, among others. Each method generates different SMLM data with quantifiable detection rates, including false negatives and positives, localization accuracies, and spatial resolutions. The usability (computational costs and interface) and speed of different algorithms should also be taken into account. Because of this variability, multiple algorithms should be considered and trialed. Ongoing awareness of the degree, to which SMLM renderings are often affected by artifacts, are not "real" images, and are not comparable to other fluorescence images, is also important.

Partly because of the non-real nature of SMLM images, analysis often poses new challenges with many established approaches, such as those used for confocal fluorescence images, frequently proving inadequate. Inherent to the tenfold improvement in lateral resolution, SMLM provides nanometer-precise dimensions of ultrastructures and clusters and elucidates sub-diffraction distributions and intermolecular/intercluster distances. Because SMLM provides images of single-molecule

locations, it also depicts molecular-level colocalizations and interactions, even allowing for quantification of these relations as well as molecular density. This is a key advantage over conventional fluorescence imaging which lacks single-molecule sensitivity and routinely relies on detection of clustered molecules, disregarding the diffuse "background" level of fluorophores. While many image parameters can be extracted from SR images manually, in order to harness the full capabilities of SMLM in biomedical research, new standardized tools for automated big data analysis are needed. Several such tools are already available for analysis of protein clusters (Andronov et al. 2016), intermolecular interactions and the formation of higher-order molecular complexes (Caetano et al. 2015), microtubule networks (Zhang et al. 2017), three-color molecular correlation (Yin and Rothenberg 2016), and general SMLM data (Malkusch and Heilemann 2016). However, with any new research endeavor, a robust analytical approach must be devised; thus, most successful applications of SMLM will rely on collaboration with computational science and bioinformatics specialists.

14.5 Future Potential

Taking into account the many different aspects and complexities of SMLM discussed, its use remains highly specialized and challenging. In particular the highly interdisciplinary demands of SMLM require that research groups making use of the method possess a breadth of skills including optics, photophysics, photochemistry, coding, and mathematics, and the biology required to not only prepare and handle samples but to pose relevant questions. Increased interest from the biomedical research community has encouraged various microscopy companies to develop systems with integrated single-molecule capabilities, but while these commercial microscopy systems provide an impressive array of imaging modalities, they are extremely costly, especially as compared to in-house customized or standard commercial microscopy systems (Holm et al. 2014). Moreover, having a commercial SMLM setup does not assist with the more difficult aspects of devising and carrying out experiments, including optimization of sample preparation and imaging acquisition parameters and data analysis. Because these challenges are ongoing, an ability to carry out these optimizations and troubleshoot SMLM experiments is integral.

Of the various potential uses of SMLM in biomedical research, perhaps the most sought after is live-cell imaging. It is particularly difficult to generate live-cell SMLM data because typically a single SMLM image takes longer than a minute to acquire; this temporal resolution is not useful for imaging many cellular processes, and so methods which make use of far fewer frames or rolling averages are often implemented. Live-cell imaging is also limited by the fluorophores available, the majority of which are less bright, less capable of "blinking," and more likely to photobleach than the synthetic dyes used for fixed-cell imaging. This has led to continuing development of better fluorescent proteins for live-cell SMLM applications, as well as novel methods for delivery of synthetic fluorophores (Chang et al. 2012; Teng et al. 2016; Hennig et al. 2015; Kube et al. 2017).

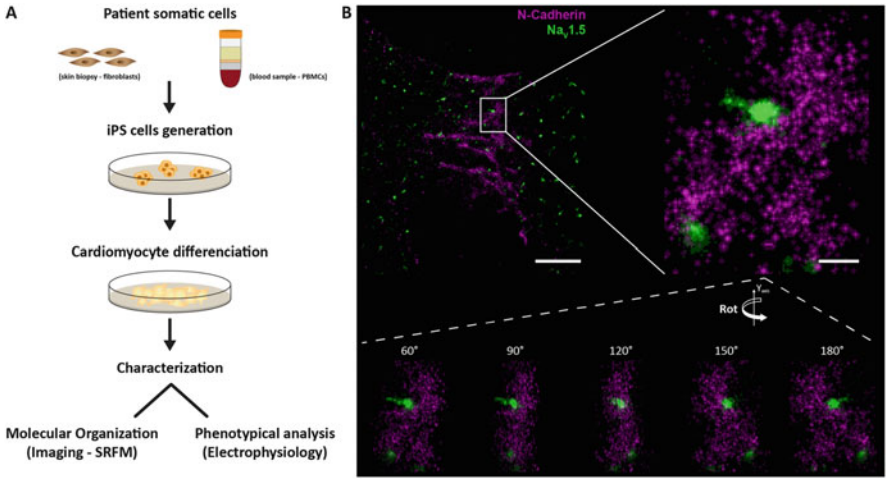

Fig. 14.5 Application of SRFM for patient-specific diagnosis. (**a**) Patient cells can be reprogrammed to pluripotent stem cells (iPS cells) and then differentiated to cardiomyocytes. These cells can then be characterized using different techniques like imaging or electrophysiology. (**b**) Human iPSC-derived cardiomyocytes analyzed by SMLM. Staining for N-cadherin (magenta) and $Na_V1.5$ (green) shows the localization of N-cadherin at regions of cell–cell contact and $Na_V1.5$ in close apposition. Scale bar: 4 μm (**b** left), 400 nm (**b** right)

Despite the difficulties associated with establishing and applying SRFM methods within the lab, the potential insights afforded by these new and exciting techniques unquestionably make their uptake worth the effort. Aside from the specific applications of SMLM to cardiac research that we have outlined in this chapter, many other successful applications to biomedical research can be found in the literature. Moreover, SMLM has potential clinical applications and has already been used in personalized disease modeling. Te Riele et al. used SMLM to assess the molecular basis for arrhythmogenic cardiomyopathy in induced pluripotent stem cell-derived cardiomyocytes generated from peripheral blood mononuclear cells from a patient carrying a *SCN5A* mutation (Fig. 14.5) (Te Riele et al. 2017). Using SMLM, they demonstrated a reduction in the number of sodium channel clusters at junctional sites, which correlated with a reduced sodium current. A reduction in the number of N-cadherin clusters was also observed at the junctional sites potentially revealing a noncanonical mechanism of $Na_V1.5$ to alter intercellular adhesion that can lead to an AC phenotype. This study, along with the others presented here, highlights the vast future potential of SMLM, spanning fundamental and biomedical research and even opening new avenues of investigation in translational and clinical medicine.

Acknowledgments The authors acknowledge the help and critical discussions with members of the Rothenberg and Delmar labs.

Compliance with Ethical Standards

Sources of Funding Work in the Rothenberg lab is funded by the NIH grants R01-GM057691 and R21-CA187612 and the American Cancer Society grant (ACS 130304-RSG-16-241-01-DMC). Research in the Delmar lab is supported by NIH grants RO1-GM57691, RO1-HL134328, and RO1-HL136179.

Conflict of Interest Authors declare that they have no conflict of interest.

Ethical Approval This article does not contain any studies with human participants or animals performed by any of the authors.

References

Agullo-Pascual E, Reid DA, Keegan S, Sidhu M, Fenyö D, Rothenberg E, et al. Super-resolution fluorescence microscopy of the cardiac connexome reveals plakophilin-2 inside the connexin43 plaque. Cardiovasc Res. 2013;100:231–40.

Agullo-Pascual E, Lin X, Leo-Macias A, Zhang M, Liang FX, Li Z, et al. Super-resolution imaging reveals that loss of the C-terminus of connexin43 limits microtubule plus-end capture and NaV1.5 localization at the intercalated disc. Cardiovasc Res. 2014;104:371–81.

Andronov L, Lutz Y, Vonesch JL, Klaholz BP. SharpViSu: integrated analysis and segmentation of super-resolution microscopy data. Bioinformatics. 2016;32:2239–41.

Baddeley D, Jayasinghe ID, Lam L, Rossberger S, Cannell MB, Soeller C. Optical single-channel resolution imaging of the ryanodine receptor distribution in rat cardiac myocytes. Proc Natl Acad Sci U S A. 2009;106:22275–80.

Betzig E, Patterson GH, Sougrat R, Lindwasser OW, Olenych S, Bonifacino JS, et al. Imaging intracellular fluorescent proteins at nanometer resolution. Science. 2006;313:1642–5.

Caetano FA, Dirk BS, Tam JH, Cavanagh PC, Goiko M, Ferguson SS, et al. MIiSR: molecular interactions in super-resolution imaging enables the analysis of protein interactions, dynamics and formation of multi-protein structures. PLoS Comput Biol. 2015;11:e1004634.

Case LB, Baird MA, Shtengel G, Campbell SL, Hess HF, Davidson MW, et al. Molecular mechanism of vinculin activation and nanoscale spatial organization in focal adhesions. Nat Cell Biol. 2015;17:880–92.

Cerrone M, Lin X, Zhang M, Agullo-Pascual E, Pfenniger A, Chkourko Gusky H, et al. Missense mutations in plakophilin-2 cause sodium current deficit and associate with a Brugada syndrome phenotype. Circulation 2014;129:1092–1103.

Chang H, Zhang M, Ji W, Chen J, Zhang Y, Liu B, et al. A unique series of reversibly switchable fluorescent proteins with beneficial properties for various applications. Proc Natl Acad Sci U S A. 2012;109:4455–60.

Dani A, Huang B, Bergan J, Dulac C, Zhuang X. Superresolution imaging of chemical synapses in the brain. Neuron. 2010;68:843–56.

De La Fuente S, Fernandez-Sanz C, Vail C, Agra EJ, Holmstrom K, Sun J, et al. Strategic positioning and biased activity of the mitochondrial calcium Uniporter in cardiac muscle. J Biol Chem. 2016;291:23343–62.

Franke C, Sauer M, van de Linde S. Photometry unlocks 3D information from 2D localization microscopy data. Nat Methods. 2017;14:41–4.

Granzier HL, Hutchinson KR, Tonino P, Methawasin M, Li FW, Slater RE, et al. Deleting titin's I-band/A-band junction reveals critical roles for titin in biomechanical sensing and cardiac function. Proc Natl Acad Sci U S A. 2014;111:14589–94.

Heilemann M, van de Linde S, Schuttpelz M, Kasper R, Seefeldt B, Mukherjee A, et al. Subdiffraction-resolution fluorescence imaging with conventional fluorescent probes. Angew Chem Int Ed Engl. 2008;47:6172–6.

Hell SW, Wichmann J. Breaking the diffraction resolution limit by stimulated emission: stimulated-emission-depletion fluorescence microscopy. Opt Lett. 1994;19:780–2.
Hennig S, van de Linde S, Lummer M, Simonis M, Huser T, Sauer M. Instant live-cell super-resolution imaging of cellular structures by nanoinjection of fluorescent probes. Nano Lett. 2015;15:1374–81.
Hess ST, Girirajan TP, Mason MD. Ultra-high resolution imaging by fluorescence photoactivation localization microscopy. Biophys J. 2006;91:4258–72.
Holm T, Klein T, Loschberger A, Klamp T, Wiebusch G, van de Linde S, et al. A blueprint for cost-efficient localization microscopy. Chemphyschem. 2014;15:651–4.
Hou Y, Jayasinghe I, Crossman DJ, Baddeley D, Soeller C. Nanoscale analysis of ryanodine receptor clusters in dyadic couplings of rat cardiac myocytes. J Mol Cell Cardiol. 2015;80: 45–55.
Huang B, Wang W, Bates M, Zhuang X. Three-dimensional super-resolution imaging by stochastic optical reconstruction microscopy. Science. 2008;319:810–3.
Huang B, Bates M, Zhuang X. Super-resolution fluorescence microscopy. Annu Rev Biochem. 2009;78:993–1016.
Jayasinghe ID, Baddeley D, Kong CH, Wehrens XH, Cannell MB, Soeller C. Nanoscale organization of junctophilin-2 and ryanodine receptors within peripheral couplings of rat ventricular cardiomyocytes. Biophys J. 2012;102:L19–21.
Johnson E, Seiradake E, Jones EY, Davis I, Grunewald K, Kaufmann R. Correlative in-resin super-resolution and electron microscopy using standard fluorescent proteins. Sci Rep. 2015;5:9583.
Kanchanawong P, Shtengel G, Pasapera AM, Ramko EB, Davidson MW, Hess HF, et al. Nanoscale architecture of integrin-based cell adhesions. Nature. 2010;468:580–4.
Kube S, Hersch N, Naumovska E, Gensch T, Hendriks J, Franzen A, et al. Fusogenic liposomes as nanocarriers for the delivery of intracellular proteins. Langmuir. 2017;33(4):1051–9.
Langhorst MF, Schaffer J, Goetze B. Structure brings clarity: structured illumination microscopy in cell biology. Biotechnol J. 2009;4:858–65.
Leo-Macias A, Agullo-Pascual E, Sanchez-Alonso JL, Keegan S, Lin X, Arcos T, et al. Nanoscale visualization of functional adhesion/excitability nodes at the intercalated disc. Nat Commun. 2016;7:10342.
Loschberger A, Franke C, Krohne G, van de Linde S, Sauer M. Correlative super-resolution fluorescence and electron microscopy of the nuclear pore complex with molecular resolution. J Cell Sci. 2014;127:4351–5.
Lukyanenko YO, Younes A, Lyashkov AE, Tarasov KV, Riordon DR, Lee J, et al. Ca(2+)/calmodulin-activated phosphodiesterase 1A is highly expressed in rabbit cardiac sinoatrial nodal cells and regulates pacemaker function. J Mol Cell Cardiol. 2016;98:73–82.
Macquaide N, Tuan HT, Hotta J, Sempels W, Lenaerts I, Holemans P, et al. Ryanodine receptor cluster fragmentation and redistribution in persistent atrial fibrillation enhance calcium release. Cardiovasc Res. 2015;108:387–98.
Malkusch S, Heilemann M. Extracting quantitative information from single-molecule super-resolution imaging data with LAMA—LocAlization microscopy Analyzer. Sci Rep. 2016;6:34486.
Munro ML, Jayasinghe ID, Wang Q, Quick A, Wang W, Baddeley D, et al. Junctophilin-2 in the nanoscale organisation and functional signalling of ryanodine receptor clusters in cardiomyocytes. J Cell Sci. 2016;129:4388–98.
Paez-Segala MG, Sun MG, Shtengel G, Viswanathan S, Baird MA, Macklin JJ, et al. Fixation-resistant photoactivatable fluorescent proteins for CLEM. Nat Methods 2015;12:215–218, 214 p following 218
Proppert S, Wolter S, Holm T, Klein T, van de Linde S, Sauer M. Cubic B-spline calibration for 3D super-resolution measurements using astigmatic imaging. Opt Express. 2014;22:10304–16.
Reid DA, Rothenberg E (2015) Single-molecule fluorescence imaging techniques. In: Encyclopedia of analytical chemistry, pp 1–20.
Rust MJ, Bates M, Zhuang X. Sub-diffraction-limit imaging by stochastic optical reconstruction microscopy (STORM). Nat Methods. 2006;3:793–5.

Sage D, Kirshner H, Pengo T, Stuurman N, Min J, Manley S, et al. Quantitative evaluation of software packages for single-molecule localization microscopy. Nat Methods. 2015;12:717–24.
Shtengel G, Galbraith JA, Galbraith CG, Lippincott-Schwartz J, Gillette JM, Manley S, et al. Interferometric fluorescent super-resolution microscopy resolves 3D cellular ultrastructure. Proc Natl Acad Sci U S A. 2009;106:3125–30.
Szymborska A, de Marco A, Daigle N, Cordes VC, Briggs JA, Ellenberg J. Nuclear pore scaffold structure analyzed by super-resolution microscopy and particle averaging. Science. 2013;341: 655–8.
Tang AH, Chen H, Li TP, Metzbower SR, MacGillavry HD, Blanpied TA. A trans-synaptic nanocolumn aligns neurotransmitter release to receptors. Nature. 2016;536:210–4.
Te Riele AS, Agullo-Pascual E, James CA, Leo-Macias A, Cerrone M, Zhang M, et al. Multilevel analyses of SCN5A mutations in arrhythmogenic right ventricular dysplasia/cardiomyopathy suggest non-canonical mechanisms for disease pathogenesis. Cardiovasc Res. 2017;113: 102–11.
Teng KW, Ishitsuka Y, Ren P, Youn Y, Deng X, Ge P, et al. Labeling proteins inside living cells using external fluorophores for microscopy. elife. 2016;5
Veeraraghavan R, Lin J, Hoeker GS, Keener JP, Gourdie RG, Poelzing S. Sodium channels in the Cx43 gap junction perinexus may constitute a cardiac ephapse: an experimental and modeling study. Pflugers Archiv Eur J Physiol. 2015;467:2093–105.
Veeraraghavan R, Lin J, Keener JP, Gourdie R, Poelzing S. Potassium channels in the Cx43 gap junction perinexus modulate ephaptic coupling: an experimental and modeling study. Pflugers Archiv Eur J Physiol. 2016;468:1651–61.
Wagner E, Lauterbach MA, Kohl T, Westphal V, Williams GS, Steinbrecher JH, et al. Stimulated emission depletion live-cell super-resolution imaging shows proliferative remodeling of T-tubule membrane structures after myocardial infarction. Circ Res. 2012;111:402–14.
Wang W, Landstrom AP, Wang Q, Munro ML, Beavers D, Ackerman MJ, et al. Reduced junctional Na+/Ca2+-exchanger activity contributes to sarcoplasmic reticulum Ca2+ leak in junctophilin-2-deficient mice. Am J Phys Heart Circ Phys. 2014;307:H1317–26.
Whelan DR, Bell TD. Super-resolution single-molecule localization microscopy: tricks of the trade. J Phys Chem Lett. 2015;6:374–82.
Wilhelm BG, Mandad S, Truckenbrodt S, Krohnert K, Schafer C, Rammner B, et al. Composition of isolated synaptic boutons reveals the amounts of vesicle trafficking proteins. Science. 2014;344:1023–8.
Wong J, Baddeley D, Bushong EA, Yu Z, Ellisman MH, Hoshijima M, et al. Nanoscale distribution of ryanodine receptors and caveolin-3 in mouse ventricular myocytes: dilation of T-tubules near junctions. Biophys J. 2013;104:L22–4.
Xu K, Zhong G, Zhuang X. Actin, spectrin, and associated proteins form a periodic cytoskeletal structure in axons. Science. 2013;339:452–6.
Yin Y, Rothenberg E. Probing the spatial organization of molecular complexes using triple-pair-correlation. Sci Rep. 2016;6:30819.
Zhang Z, Nishimura Y, Kanchanawong P. Extracting microtubule networks from superresolution single-molecule localization microscopy data. Mol Biol Cell. 2017;28:333–45.